Electronic Supplementary Material (ESI) for Environmental Science: Water Research & Technology.

Optimization of batch and packed-bed column Cr (VI) adsorption of an amine-rich chitosan/polyethyleneimine composite: Application in electroplating wastewater treatment

Ali Ansari [aϕ], *Raynara Maria Silva Jacovone* [aϕ], *Enrico Tapire Nadres* [a], *Minh Đỗ* [a], *Debora Frigi Rodrigues* [a*]

[a] Department of Civil and Environmental Engineering, Room N136 Engineering Building 1, University of Houston, TX 77204-4003 (U.S.A.)

ϕ Equal contribution

[*]Corresponding Author: Email: dfrigirodrigues@uh.edu; Phone: +1-713-743-1495

Materials:

Chitosan, glutaraldehyde (25%), hydrochloric acid (37%), potassium dichromate (≥99%), and sodium chloride (≥99%) were purchased from Sigma-Aldrich Inc. Polyethyleneimine (M_n=60,000, M_w=750,000) solution (50%), sodium bicarbonate, sodium hydroxide, and sodium sulfate anhydrous were purchased from Fisher Scientific. No further purification was done on the chemicals, and they were used as received. Deionized water was used to prepare the solutions.

CS-PEI-GLA characterization:

The prepared adsorbent was characterized by Attenuated Total Reflectance Fourier Transform Infrared spectroscopy (ATR-FTIR) in the 4000-800 cm^{-1} range with a 4 cm^{-1} resolution. X-ray photoelectron spectroscopy (XPS) was performed at high and low resolutions with pass energies of 23.5 and 187.85 eV. Scanning Electron Microscopy (SEM) images were taken by JEOL JSM 6400 after coating the samples with gold.

Batch experiments:

To optimize the concentration of PEI in the absorbent, four adsorbents with 0%, 2%, 5%, and 10% PEI were prepared. A mass of 20 mg of CS-PEI-GLA was put into contact with 40 mL Cr (VI) solution (250 mg/L) at pH=7. Samples were taken from each mixture after 16 h. For the effect of pH, 20 mg of CS-PEI-GLA with optimized PEI concentration (10%) was mixed with 20 mL of 100 mg/L chromium (VI) solutions with a wide range of pH from 2 to 10. The pH adjustment was done using sodium hydroxide (0.1 M) or hydrochloric acid (0.1 M), and the mixtures were shaken for 16 h. For the effect of dosage, 20 mL of 100 mg/L Cr (VI) was mixed with different amounts of optimized CS-PEI-GLA (10, 20, 50, 75, 100, 125, 250 mg) at pH=7. Then the mixtures were shaken for 16 h. For the effect of time and to determine kinetic models

governing the adsorption process, 25 mg of the optimized adsorbent was added to 50 mL solutions containing 50, 100, and 250 mg/L Cr (VI) at pH=7. An aliquot of 1 mL sample was taken from each solution after 2, 7, 15, 45, 90, 960 min and analyzed for chromium concentration. The data obtained from the previous tests were used to design the experiment for investigating how Cr (VI) concentration affects adsorption capacity. Five different concentrations were used: 20, 50, 100, 250, and 500 mg/L. A mass of 25 mg of the optimized CS-PEI-GLA was added to 50 mL solution at pH=7 for each initial concentration. The samples were shaken for 2 h. To investigate the temperature's effect, a mass of 25 mg of CS-PEI-GLA was added to 50 mL of 100 mg/L Cr (VI) at pH=7 at four different temperatures (20, 30, 40, and 50 ºC). Samples were shaken (120 rpm) for 2 h. For the coexisting ions experiment, 25 mg of CS-PEI-GLA was added to 50 mL solution of 100 mg/L Cr (VI) and Cl^-, NO_3^-, SO_4^{2-}, PO_4^{3-} in a range of concentration from 200 to 2000 mg/L and Cd^{2+} and Zn^{2+} in a range of concentration 20 to 2000 [1, 2] at pH=7. Samples were shaken (120 rpm) for 2 h.

Column details and parameters:

The column setup consisted of a glass cylinder with an inner diameter of 1.5 cm and 30 cm height. The optimized adsorbent in the batch process was packed into the column and soaked in deionized water overnight. Cr (VI) solution was pumped to the top of the column by a peristaltic pump. From the bottom of the column, effluent samples (25 mL) were collected. Chromium concentration was measured by AAS overtime until the column became saturated as described in section 2.2. The highest chromium removal was achieved by optimizing the flow rate, influent concentration of Cr (VI), and bed height. The effect of these three parameters on the breakthrough curve, breakthrough time t_b (min), experimental adsorption capacity q_{exp} (mg/g),

and the volume of clean water obtained before breakthrough point V_b (mL) were investigated. The description of these parameters is provided below:

(a) breakthrough time t_b (min) is the time at the breakthrough point where C_{eff}=0.1 C_{inf} [1], where C_{inf} and C_{eff} (mg/L) are the Cr (VI) concentration in influent and effluent, respectively,

(b) experimental adsorption capacity q_{exp} (mg/g),

$$q_{exp} = \frac{QC_{inf}\int_{t=0}^{t=total}(1-\frac{C_{eff}}{C_{inf}})dt}{M}$$

Equation (S1)

where t (min) is the time, Q (L/min) is the flow rate, and M (g) is the adsorbent mass,

(c) total effluent volume up to the breakthrough point, V_b (mL),

$$V_b = Qt_b$$ Equation (S2)

Mathematical modeling

Kinetic models

The data collected from the experiments with three different initial concentrations of Cr (VI) and sampling over time was used to calculate the parameters for two kinetic models, namely pseudo-first order (**Eq. S3**) and pseudo-second order (**Eq. S4**) [2, 3].

$$q_t = q_e(1 - e^{-k_1 t})$$ Equation (S3)

where q_{eq} (mg/g) is the adsorption capacity at the equilibrium, q_t (mg/g) is the adsorption capacity at time t (min), and k_1 (1/min) is the rate constant for pseudo-first order model.

$$q_t = \frac{q_e^2 k_2 t}{1 + q_e k_2 t}$$

Equation (S4)

k_2 (g/mg.min) is the second-order rate constant.

Isotherms

The obtained data from the effect of initial concentration of Cr (VI) on adsorption was used to determine model parameters for Langmuir (**Eq. S5**), Freundlich (**Eq. S6**), Redlich-Peterson (Eq. S7), Sips (Eq. S8), and Toth (Eq. S9) isotherm models by nonlinear regression [4, 5].

$$\frac{q_{eq}}{q_{max}} = \frac{K_L C_e}{1 + K_L C_e}$$

Equation (S5)

maximum adsorption capacity is presented by q_{max} (mg/g), and K_L (L/mg) is the constant for Langmuir model,

$$q_{eq} = K_F C_e^{1/n}$$

Equation (S6)

where K_F (L/g) is the Freundlich constant and 1/n is the sorption intensity,

$$q_{eq} = \frac{A_{RP} C_e}{1 + B_{RP} C_e^{\,g}}$$

Equation (S7)

where A_{RP} (L/g), B_{RP} ((L/mg)^g), and g are the Redlich-Peterson's model constants,

$$q_{eq} = \frac{q_s (K_s C_e)^{1/n_s}}{1 + (K_s C_e)^{1/n_s}}$$

Equation (S8)

where q_s (mg/g), K_s (L/mg), and n_s are the Sips' model constants,

$$q_{ea} = \frac{q_t K_t C_e}{(1 + (K_t C_e)^t)^{1/t}}$$

Equation (S9)

where q_t (mg/g), K_t (L/mg), and t are the Toth's model constants.

Breakthrough models

The simplified forms of packed-bed column breakthrough models that are commonly being used in environmental adsorption studies *i.e.* Bohart-Adams, Thomas, and Yoon-Nelson are mathematically identical [6, 7]. Hence, first the data obtained from experiments were fitted to the standard logistic function (**Eq. S10**) to determine its parameters, then parameters associated to each of these three models were calculated following **Table S1**.

$$\frac{C_{eff}}{C_{inf}} = \frac{1}{1 + exp(a - bt)}$$

Equation (S10)

the parameters of the logistic function are presented by a (dimensionless) and b (1/min). The breakthrough models' parameters can enhance our knowledge about the adsorption process in the column.

Table S1: Breakthrough models' parameters

Model	Parameters	Logistic	Logistic
Thomas	K_{Th}, q_m	$\frac{K_{Th} q_m M}{Q}$	$K_{Th} C_0$

Bohart-Adams	K_{B-A}, N_m	$\frac{K_{B-A}N_mH}{u}$	$K_{B-A}C_0$
Yoon-Nelson	K_{Y-N}, τ	$K_{Y-N}\tau$	K_{Y-N}

K_{Th} (L/mg.min) is the Thomas rate constant, q_m (mg/g) is the model adsorption capacity per unit mass of CS-PEI-GLA, K_{B-A} (L/mg.min) is the Bohart-Adams rate constant, N_m (mg/L) is the model adsorption capacity per unit volume of the bed, H is the height of the bed (cm), u (cm/min) is the linear velocity, K_{Y-N} (1/min) is Yoon-Nelson rate constant, and τ (min) is the time when adsorbate reaches to half of the breakthrough.

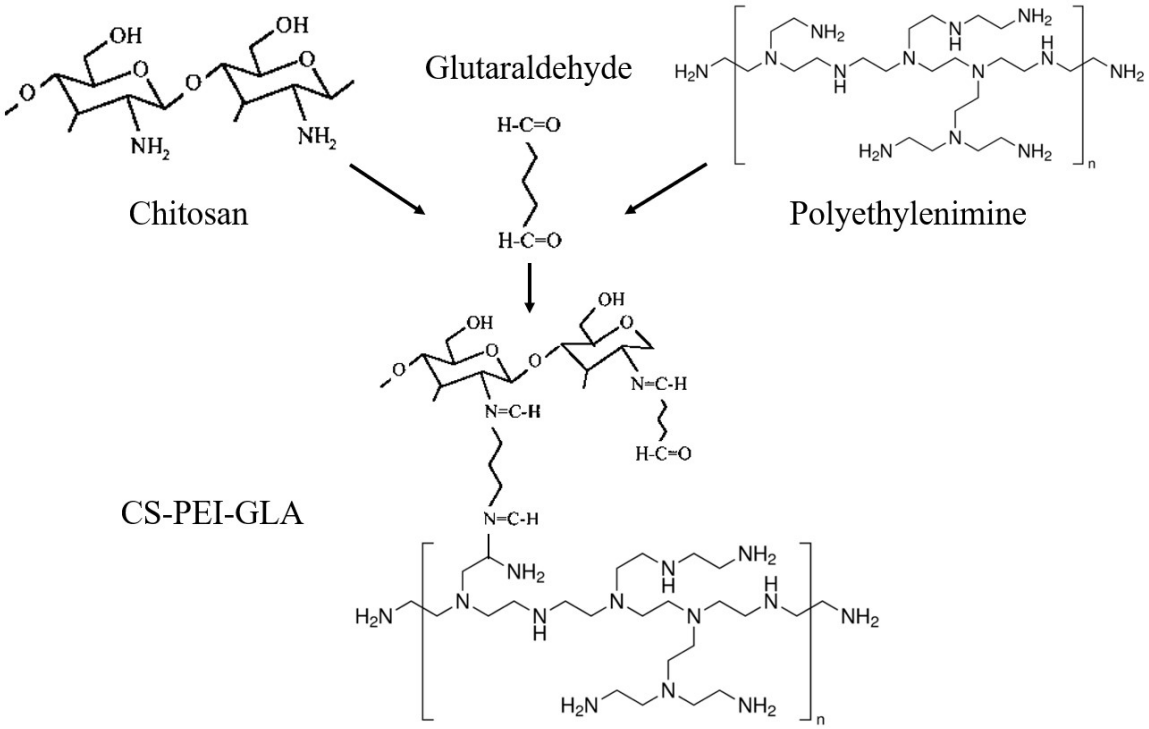

Figure S1: Schematic representation of the crosslinking of chitosan and polyethyleneimine with glutaraldehyde.

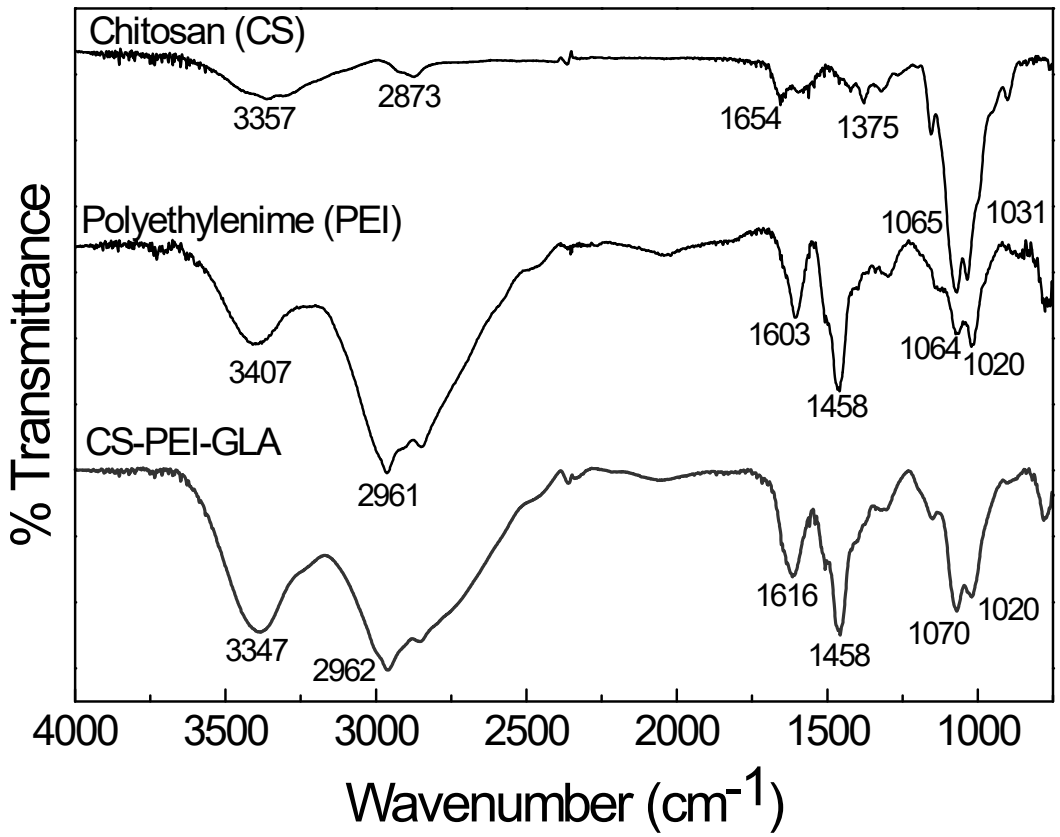

Figure S2: ATR-FTIR spectra of the starting materials, CS and PEI, and the product CS-PEI-GLA composite used in the adsorption of nitrate (adapted from Nadres *et al.* [8])

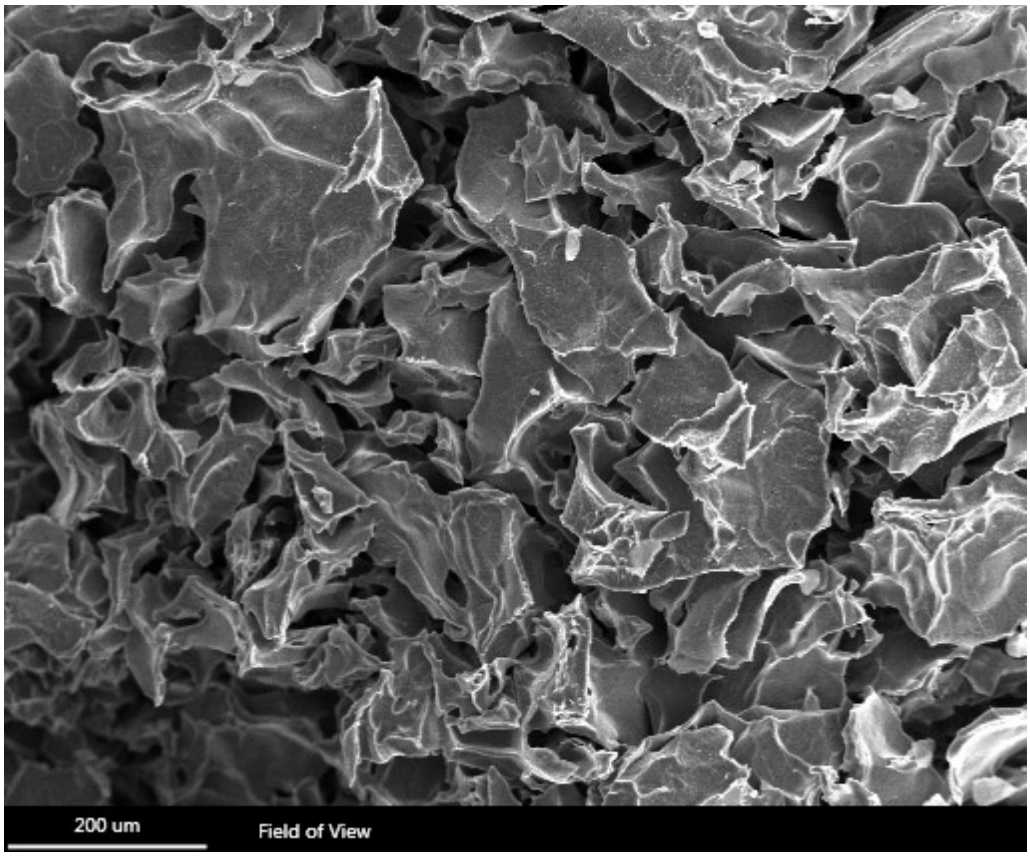

Figure S3: SEM image of the freeze-dried CS-PEI-GLA adsorbent (adapted from Nadres *et al.* [8])

Table S2: XPS analysis of the elemental composition of the four adsorbents

Sample	Elements concentration (%)		
	C	N	O
CS-PEI 0%-GLA	72.2	5	22.8
CS-PEI 2%-GLA	76.2	7.4	16.4
CS-PEI 5%-GLA	74.9	12.8	12.3
CS-PEI 10%-GLA	78	15.4	6.6

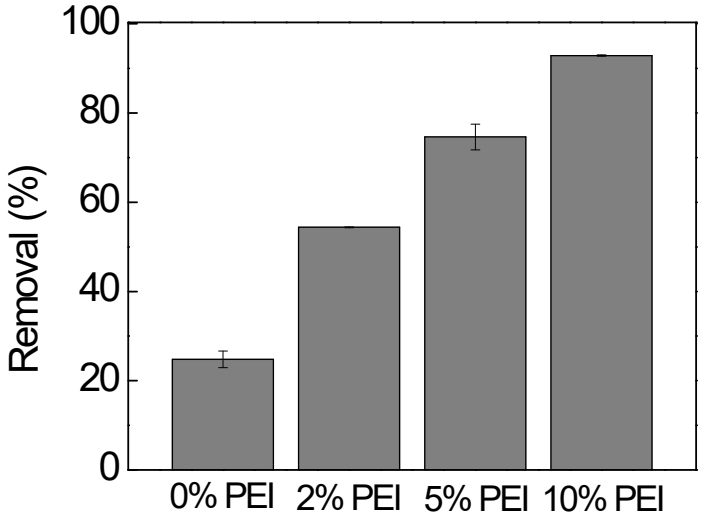

Figure S4: Effect of PEI content in the adsorbents on Cr (VI) removal. 20 mg of each adsorbent was added to a 40 mL solution containing 250 mg/L of Cr (VI). The error bars represent standard deviations calculated from triplicate experiments.

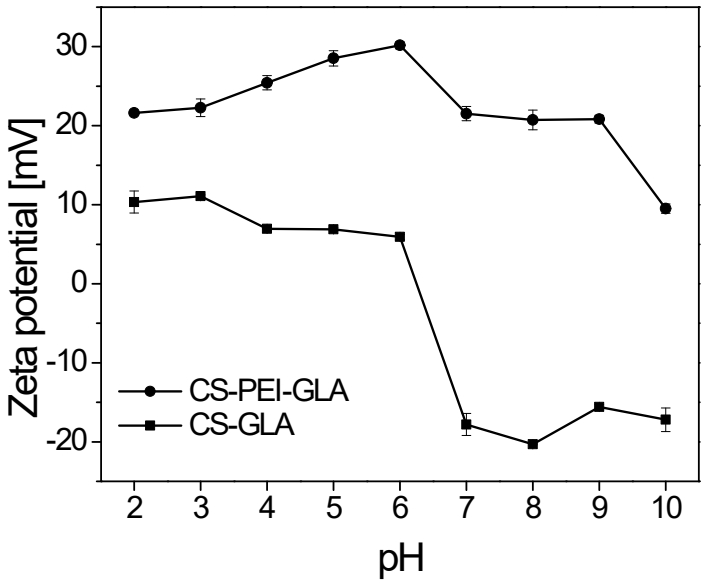

Figure S5: Zeta potential of CS-PEI-GLA and CS-GLA adsorbent at different pH (adapted from Nadres *et al.* [9])

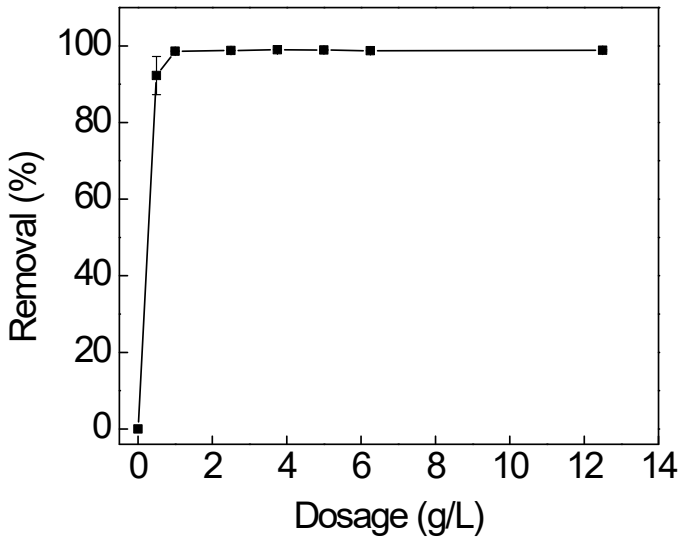

Figure S6: (a) Effect of CS-PEI-GLA dosage on Cr (VI) (100 mg/L) removal from a 20 mL solution at pH=7 after 16 h. The error bars represent standard deviations calculated from triplicate experiments.

Table S3: Comparison of the maximum adsorption capacity of Cr (VI) calculated from Langmuir model on CS-PEI-GLA with other adsorbents found in the literature

Adsorbent material	q_{max} (mg/g)	Ref.
CS-PEI-GLA	500	This study
PEI modified cocoa shell	24.78	[10]
PEI and chloroacetic acid-functionalized CS microsphere	331.32	[11]
Zirconium incorporated CS-gelatin composite	138.89	[12]
CS/activated carbon/magnetite	130.80	[13]
CS coated with poly 3-methyl thiophene	127.62	[14]
Amberlite IRA-743 resin	306.60	[15]
Amine-functionalized cellulose nanofiber-sodium alginate-Fe(III)	526.32	[16]
Carbon dots-incorporated fluorescent nanocellulose aerogels	543.38	[17]
Sulfur quantum dots embedded in chitosan hydrogels	186.22	[18]

Thermodynamics

Equations S11 to 13 [59]:

$$\Delta G^o = \Delta H^o - T\Delta S \quad \text{Equation (S11)}$$

$$k_d = \frac{Q_e}{C_e} \quad \text{Equation (S12)}$$

$$\ln k_d = \frac{\Delta S^o}{R} - \frac{\Delta H^o}{RT} \quad \text{Equation (S13)}$$

where T is the temperature in Kelvin (K); and R is the universal gas constant, 8.314 (J K/mol); k_d is the partition coefficient; Q_e is the equilibrium concentration of metal ions on the adsorbent (mg/g), and C_e is the equilibrium concentration of metal ions in the solution (mg/L).

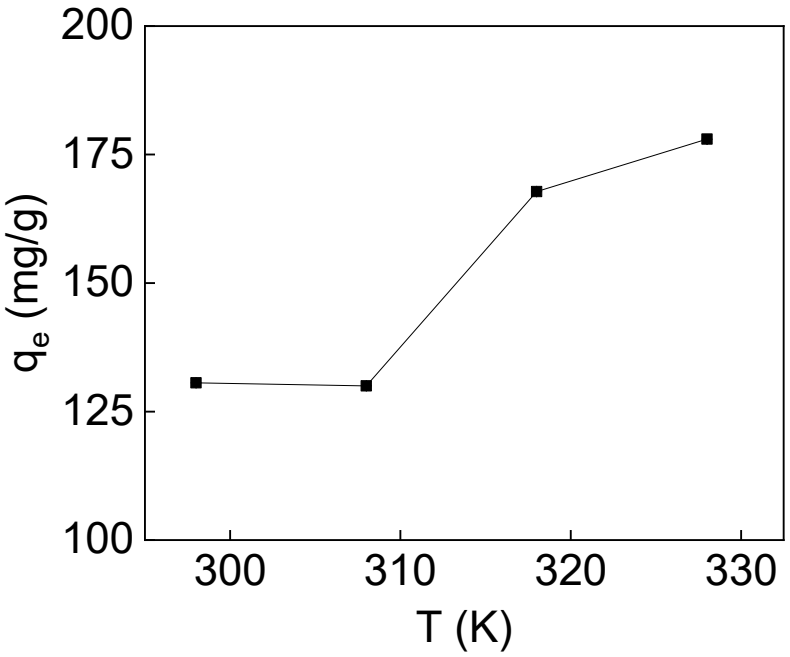

Figure S7: The effect of temperature on the Cr (VI) adsorption. Experiments were performed at pH 7 with 100 ppm Cr (VI) solution at four different temperatures (20, 30, 40, and 50 ºC). The standard deviation based on triplicate experiments are represented by the error bars.

The values of ΔH° and ΔS° were calculated, respectively, from the Van't Hoff plot slope and intercept as shown in Figure S6.

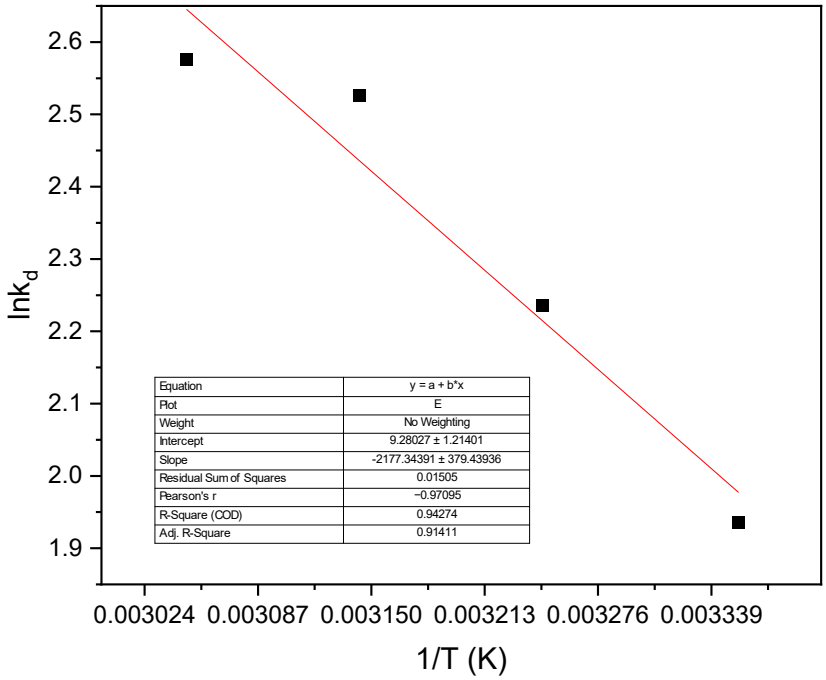

Figure S8: Van't Hoff plot slope.

Table S4: Thermodynamic parameters for Cr (VI) adsorption on CS-PEI-GLA.

Temperature (K)	**k_d**	**ΔG° (kJ/mol)**	**ΔH° (kJ/mol)**	**ΔS° (J/K. mol)**
298	6.91	-4.90	18.10	77.16
308	9.32	-5.67		
318	12.47	-6.45		
328	13.10	-7.21		

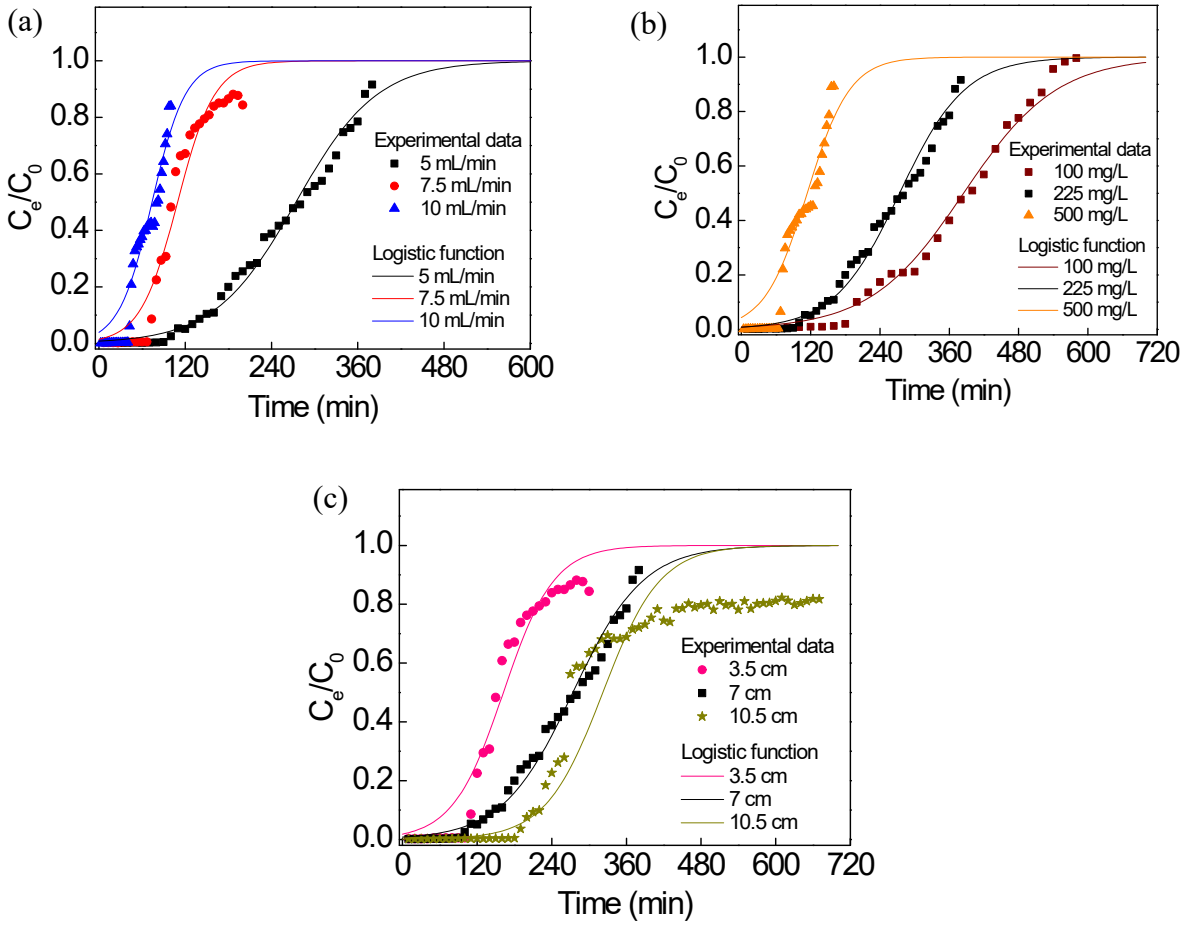

Figure S9: Breakthrough curves for Cr (VI) with the column packed with CS-PEI-GLA at different conditions. (a) Effect of flow rate, (b) effect of initial concentration, and (c) effect of bed height.

Table S5: Parameters determination of Bohart-Adams, Thomas, and Yoon-Nelson models

Run #	R^2	K_{BA}, K_{Th} * 10^{-5} (L/mg.min)	N_m (mg/L)	q_m (mg/g)	K_{YN} * 10^{-2} (1/min)	τ (min)
1	0.9743	7.8	1495.97	616.53	1.77	274.01
2	0.9571	17.2	895.30	368.98	3.86	109.33
3	0.9458	19.2	806.95	332.56	4.33	73.90
4	0.9831	12.4	933.40	384.68	1.24	384.68
5	0.9478	5.4	1383.34	570.11	2.71	114.02
6	0.9504	10.9	1771.01	729.88	2.46	162.20
7	0.8407	9.6	1172.41	483.18	2.17	322.12

R^2 is the goodness-of-fit, $K_{B\text{-}A}$ (L/mg.min) is the rate constant for Bohart-Adams model, K_{Th} (L/mg.min) is the rate constant for Thomas model, q_m (mg/g) is the mass adsorption capacity from Thomas model, N_m (mg/L) is the volume adsorption capacity from Bohart-Adams model, $K_{Y\text{-}N}$ (1/min) is the rate constant for Yoon-Nelson model, and τ (min) represent the time at half of the breakthrough.

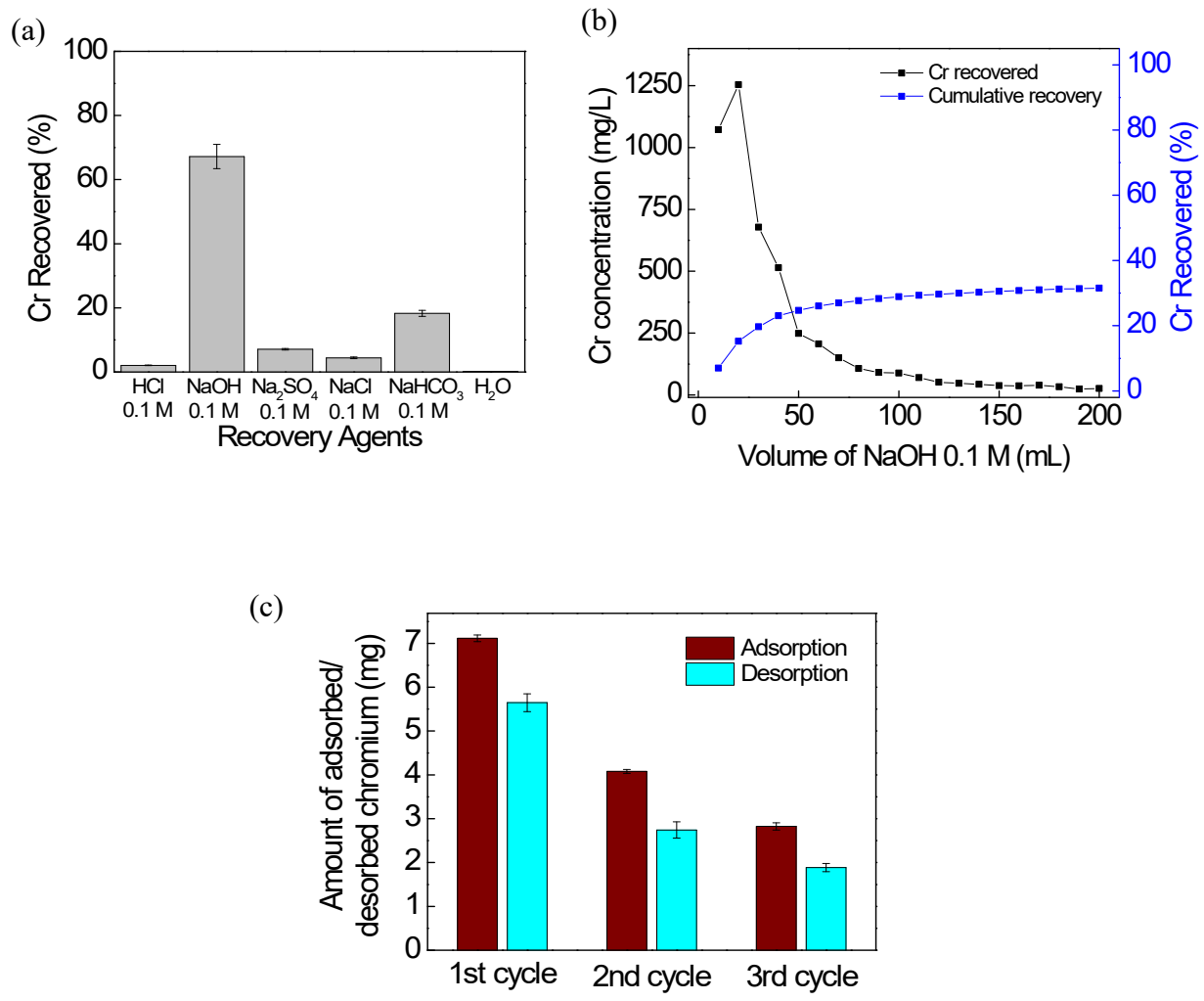

Figure S10: (a) Recovery of chromium from 20 mg saturated CS-PEI-GLA with 40 mL of different agents in batch. (b) Chromium concentration in the effluent and cumulative recovery of chromium from saturated column (7 cm) by 200 mL of NaOH 0.1 M at 5 mL/min. (c) The adsorbed/desorbed amount of chromium to/from the adsorbent in three cycles with NaOH 0.1 M as recovery agent.

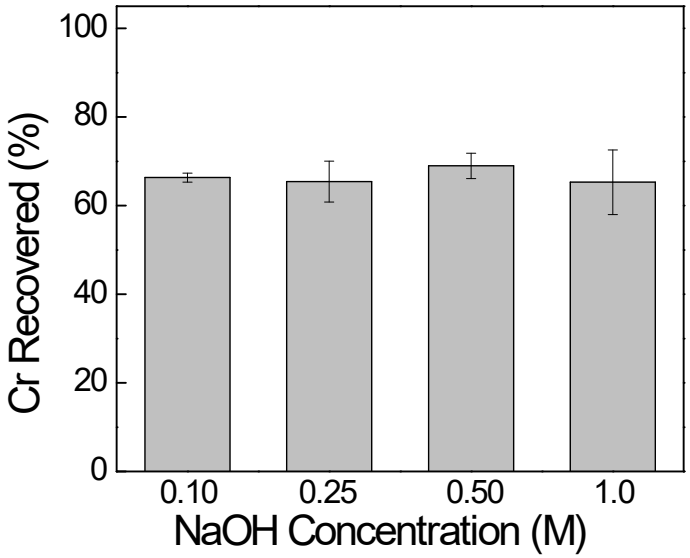

Figure S11: Effect of NaOH concentration on recovery of chromium ions from CS-PEI-GLA

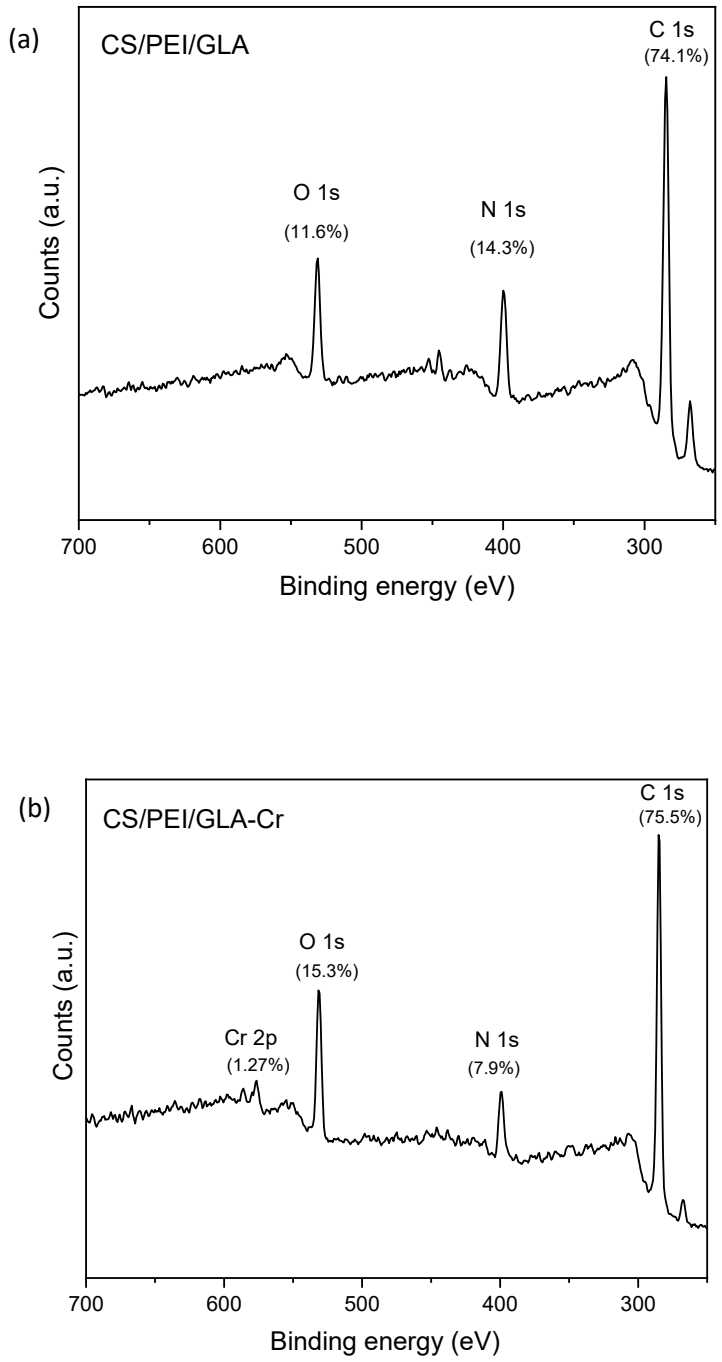

Figure S12: XPS spectra of the survey (a) before and (b) after Cr (VI) removal. Experiments were performed at pH 7 with 100 ppm Cr (VI).

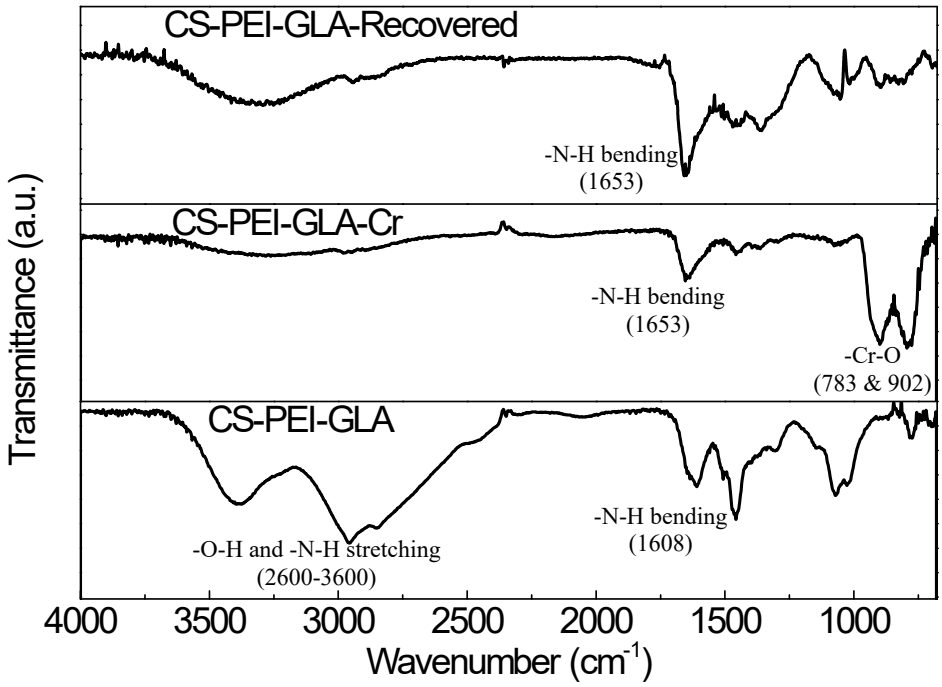

Figure S13: FTIR spectra of the adsorbent before adsorption (CS-PEI-GLA), adsorbent after chromium adsorption (CS-PEI-GLA-Cr), and adsorbent after recovery with NaOH 0.1 M (CS-PEI-GLA-Recovered).

Table S6: Allied Plating wastewater characteristics

pH	4.88
Total Cr, mg/L	263
TSS, mg/L	384
TDS, mg/L	608
TOC, mg/L	20
COD, mg/L	167

References

1. González-López, M.E., et al., *Fixed-bed adsorption of Cr(VI) onto chitosan supported on highly porous composites.* Environmental Technology & Innovation, 2020. **19**: p. 100824.
2. Ansari, A., et al., *Novel Fe3O4/hydroxyapatite/β-cyclodextrin nanocomposite adsorbent: Synthesis and application in heavy metal removal from aqueous solution.* 2019. **33**(1): p. e4634.
3. Bandara, P., et al., *Graphene oxide nanocomposite hydrogel beads for removal of selenium in contaminated water.* ACS Applied Polymer Materials, 2019.
4. Bandara, P.C., et al., *Graphene Oxide Nanocomposite Hydrogel Beads for Removal of Selenium in Contaminated Water.* ACS Applied Polymer Materials, 2019. **1**(10): p. 2668-2679.
5. Brdar, M., et al., *Comparison of two and three parameters adsorption isotherm for Cr(VI) onto Kraft lignin.* Chemical Engineering Journal, 2012. **183**: p. 108-111.
6. Hu, Q., et al., *Fractal-like kinetics of adsorption on heterogeneous surfaces in the fixed-bed column.* Chemical Engineering Journal, 2019. **358**: p. 1471-1478.
7. Chu, K.H., *Breakthrough curve analysis by simplistic models of fixed bed adsorption: In defense of the century-old Bohart-Adams model.* Chemical Engineering Journal, 2020. **380**: p. 122513.
8. Nadres, E.T., J.V.D. Perez, and D.F.J.P.o.t.W.E.F. Rodrigues, *High-capacity hydrogel polymer composite adsorbent for nitrate and phosphate removal from water.* 2017. **2017**(3): p. 438-460.
9. Nadres, E.T., J.V.D. Perez, and D.F. Rodrigues, *High-capacity hydrogel polymer composite adsorbent for nitrate and phosphate removal from water.* Proceedings of the Water Environment Federation, 2017(3): p. 438-460.
10. Fotsing, P.N., et al., *Surface modification of biomaterials based on cocoa shell with improved nitrate and Cr(vi) removal.* RSC Advances, 2020. **10**(34): p. 20009-20019.
11. Zhu, W., et al., *Cr(VI) and Pb(II) capture on pH-responsive polyethyleneimine and chloroacetic acid functionalized chitosan microspheres.* Carbohydrate Polymers, 2019. **219**: p. 353-367.
12. Preethi, J., et al., *Facile synthesis of Zr4+ incorporated chitosan/gelatin composite for the sequestration of Chromium(VI) and fluoride from water.* Chemosphere, 2021. **262**: p. 128317.
13. Bahador, F., et al., *Enhancement of the chromium removal behavior of Moringa oleifera activated carbon by chitosan and iron oxide nanoparticles from water.* Carbohydrate Polymers, 2021. **251**: p. 117085.
14. Hena, S., *Removal of chromium hexavalent ion from aqueous solutions using biopolymer chitosan coated with poly 3-methyl thiophene polymer.* Journal of Hazardous Materials, 2010. **181**(1): p. 474-479.
15. Polowczyk, I., et al., *Equilibrium and kinetic study of chromium sorption on resins with quaternary ammonium and N-methyl-d-glucamine groups.* Chemical Engineering Journal, 2016. **284**: p. 395-404.
16. Hu, Z., et al., *Amine-functionalized cellulose nanofiber-sodium alginate-Fe(III) porous hollow beads for the efficient removal of Cr(VI).* Cellulose, 2023. **30**(6): p. 3807-3822.

17. Wang, H., et al., *Visualized adsorption and enhanced photocatalytic removal of Cr6+ by carbon dots-incorporated fluorescent nanocellulose aerogels.* International Journal of Biological Macromolecules, 2023. **253**: p. 127206.
18. Deng, S., et al., *Simultaneous Detection and Adsorptive Removal of Cr(VI) Ions by Fluorescent Sulfur Quantum Dots Embedded in Chitosan Hydrogels.* ACS Applied Nano Materials, 2023. **6**(3): p. 1817-1827.